HAL
open science

Calculation of the dynamic response of a viscoelastic railway structure based on a quasi-stationary approach

Olivier Chupin, Antoine Martin, Jean Michel Piau, Pierre-Yves Hicher

To cite this version:

Olivier Chupin, Antoine Martin, Jean Michel Piau, Pierre-Yves Hicher. Calculation of the dynamic response of a viscoelastic railway structure based on a quasi-stationary approach. International Journal of Solids and Structures, 2014, 51 (13), pp.2297-2307. 10.1016/j.ijsolstr.2014.02.035 . hal-01630720

HAL Id: hal-01630720

https://hal.science/hal-01630720v1

Submitted on 2 Dec 2017

HAL is a multi-disciplinary open access archive for the deposit and dissemination of scientific research documents, whether they are published or not. The documents may come from teaching and research institutions in France or abroad, or from public or private research centers.

L'archive ouverte pluridisciplinaire **HAL**, est destinée au dépôt et à la diffusion de documents scientifiques de niveau recherche, publiés ou non, émanant des établissements d'enseignement et de recherche français ou étrangers, des laboratoires publics ou privés.

Calculation of the dynamic response of a viscoelastic railway structure based on a quasi-stationary approach

O. Chupin [a,*], A. Martin [a], J.-M. Piau [a], P.-Y. Hicher [b]

[a] LUNAM Université, IFSTTAR, MAST, F-44341 Bouguenais, France
[b] Research Institute in Civil and Mechanical Engineering, UMR CNRS 6183, Ecole Centrale Nantes, France

A semi-analytical method has been developed for computing the dynamic response of railways composed of viscoelastic layers under moving loads. One of the aims of this new approach is to be able to simulate railways incorporating asphalt materials. These materials are increasingly used or highly considered for construction projects. We have modeled the mechanical behavior of bituminous mixes with the Huet–Sayegh thermo-sensitive viscoelastic law that is specifically intended for such materials. This method, implemented in a numerical program, is based on a quasi-stationary approach, so that time is not a specific factor in the solution. The required calculation time is therefore small, for the convenience of parametric studies. The capability of this method is proved with a numerical example that provides several validation points and illustrates at the same time the temperature effect on the response of a railway including an asphalt layer.

Keywords:
Railway
Asphalt material
Dynamic response
Semi-analytical method
Viscoelasticity

1. Introduction

The increase of traffic volume and speed is probably going to affect the design of railways and lead to the construction of new lines possibly incorporating novel technologies (e.g. use of asphalt paving materials, structures without ballast...) whose performances need to be evaluated. In such investigations, modeling and numerical simulation of the mechanical response of railways is complementary to laboratory and on-site experimentations. This has motivated the present study for the development of a numerical program for computing the dynamic response of railway structures with a view to meeting two objectives which are: (i) the design of a program that requires small computation times (therefore, suited to parametric studies) and (ii) that is able to deal with structures incorporating layers of asphalt materials (viscoelastic), which are now highly considered for construction projects (Rose et al., 2011). To fulfill these goals, we developed a semi-analytical method which is presented thereafter.

There exist various formulations that allow the modeling of the dynamic response of railway structures under moving loads. Here we focus on analytical and semi-analytical methods that require small computation time compared to the boundary element or finite element methods which nonetheless have been used already to simulate the response of railway tracks and which are well-documented in the specialized literature. Concerning analytical and semi-analytical methods, after Vostroukhov and Metrikine (2003) one of the first models was proposed by Filippov (1961) who represented the structure by an Euler–Bernoulli beam resting on an elastic half-space. Then, improved models were developed to take into account the soil composed of elastic or viscoelastic layers, as well as the sleepers that distribute the load at the surface of the soil structure (Metrikine and Popp, 1999; Van den Broeck et al., 2002), or different types of loads (i.e. constant intensity or harmonic loads, e.g. Sheng et al., 1999). Among the cited references, Metrikine and Popp (1999) presented a pioneering analytical study of a three-dimensional non-homogeneous model for a railway track by considering an Euler–Bernoulli beam laid on periodically positioned supports resting on a elastic half-space. Vostroukhov and Metrikine (2003) presented an improvement of this model by replacing the elastic half-space by a layer of viscoelastic material (Kelvin–Voigt model) placed over a substratum. Along the same lines, the present paper presents a new method for computing the three-dimensional dynamic response of a railway track system composed of Euler–Bernoulli beams laid on sleepers resting on a multilayered structure. The latter may incorporate asphalt layers whose behavior, in contrast with previous works, is represented by a thermo-sensitive viscoelastic constitutive law specifically

* Corresponding author. Tel.: +33 240 845 786; fax: +33 240 845 994.
E-mail addresses: olivier.chupin@ifsttar.fr (O. Chupin), antoine.martin@ifsttar.fr (A. Martin), jean-michel.piau@ifsttar.fr (J.-M. Piau), pierre-yves.hicher@ec-nantes.fr (P.-Y. Hicher).

adapted to bituminous mixes, the Huet–Sayegh model (Huet, 1963; Sayegh, 1965), which is commonly used in the field of road pavement. As explained further, this method is based on a sub-structuring technique and a decomposition of the pressure distribution under the sleepers into "loading waves" which allow us to solve the problem in a quasi-stationary framework that does not require time to be explicitly accounted for. Then, we can avoid the moving of the loading on the rails. The developed method can be seen as an extension of the methods dedicated to homogeneous structures, for which the solution is sought in the moving reference frame (e.g. Frýba, 1999; Barros and Luco, 1994), to take into account the specificity of railway tracks and loading conditions.

The outlines of the paper are as follows: the first sections aim at providing the model assumptions and describing the proposed method, as well as presenting the Huet–Sayegh viscoelastic model. Then, numerical examples are presented to validate the approach and to demonstrate its capabilities to simulate dynamic effects in the structure and to account for the presence of asphalt layers.

2. Preliminary considerations

2.1. Position of the problem

The geometry and the mechanical model considered in this paper to represent the railway infrastructure are shown in Fig. 1. In order to compute the dynamic response of the railway structure to a passing train, we propose a sub-structuring procedure (or decoupling method) that consists in separating the initial model into two subsystems which are: (i) the track system which consists in rails secured on periodically positioned sleepers and (ii) the sub-structure (trackbed plus soil) modeled as a stacking of semi-infinite layers. The link between these two subsystems is made through the pressure distribution, $p(x,t)$, at the surface of the trackbed (interface between the subsystems) which is straightly correlated to the load transfer across the track system. In the numerical procedure, this pressure distribution is first set to a given initial value and an iterative process based on a fix point method is used to make the solution converge to the actual distribution corresponding to the global coupled system. The dynamic response of the sub-structure is given by the mechanical fields (stress, displacement, acceleration, etc.) obtained after convergence. In order to compute the dynamic response of the sub-structure to the pressure distribution $p(x,t)$, as required by the iterative process, we use a numerical code intended for road pavement structures and based on a quasi-stationary approach. To comply with the requirements of that program called ViscoRoute©2.0, a decomposition method of $p(x,t)$ into "loading waves" is proposed. The advantages of using ViscoRoute©2.0 are two-fold. First, the computation time is small because of the semi-analytical method considered in ViscoRoute©2.0 and the constitutive behavior of the material layers can be chosen as viscoelastic according to the Huet–Sayegh model, which is fully adapted to asphalt materials. In the next section, we present the main features of ViscoRoute©2.0.

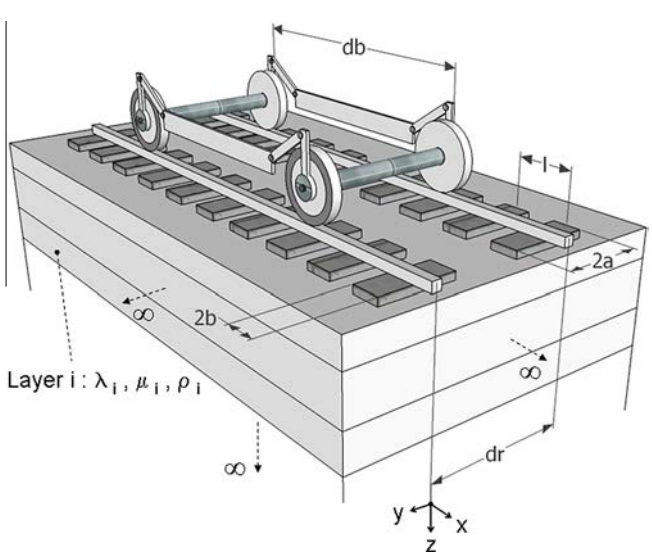

Fig. 1. Schematic representation of a portion of the railway track system under consideration submitted to a bogie comprising two axle loads and moving at constant speed.

2.2. ViscoRoute©2.0: a numerical program for the computation of the quasi-stationary response of a layered medium subjected to moving loads

This numerical code has been described in previous works, which the reader is referred to for a more comprehensive description (Duhamel et al., 2005; Chabot et al., 2010; Chupin et al., 2010). Only a summary of the main features is given in the present section.

ViscoRoute©2.0 is a numerical program designed to solve the equations of motion for semi-infinite layered media excited by loads moving at constant speed. The layers are supposed to be homogeneous and their constitutive behavior is either linear elastic or viscoelastic according to the Huet–Sayegh model, which is well suited for asphalt materials. As shown on the schematic representation in Fig. 2, this model is represented (in one dimension) by a purely elastic spring (E_0) (branch I) connected in parallel to two parabolic dampers in series with an elastic spring ($E_\infty - E_0$) (branch II). In the frequency domain in which asphalt materials are characterized, the complex modulus of the Huet–Sayegh model reads:

$$E^*(\omega\tau(\theta)) = E_0 + \frac{E_\infty - E_0}{1 + \delta(i\omega\tau(\theta))^{-k} + (i\omega\tau(\theta))^{-h}} \tag{1}$$

E_0 is the static elastic modulus, E_∞ is the instantaneous elastic modulus, k and h are exponents of the parabolic dampers ($1 > h > k > 0$), and δ is a positive non-dimensional coefficient balancing the contribution of the first damper in the global behavior. θ denotes the temperature and τ is a response time parameter which accounts for the equivalence principle between frequency and temperature. τ is governed by the following equation:

$$\tau(\theta) = \exp\left(A_0 + A_1\theta + A_2\theta^2\right) \tag{2}$$

where A_0, A_1 and A_2 are constant parameters. The extension of the Huet–Sayegh model to a tensorial expression can be obtained simply by considering a constant Poisson's ratio, υ; it reads in the frequency domain:

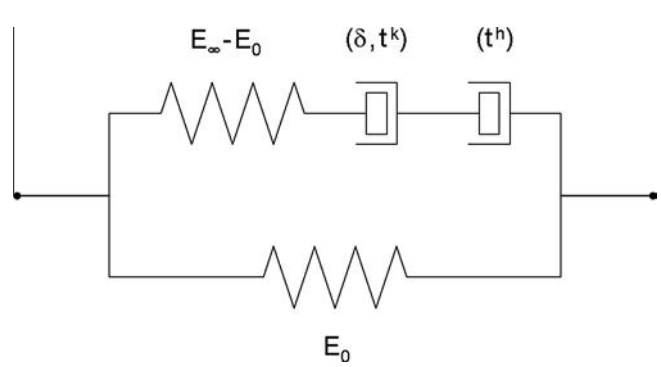

Fig. 2. Schematic representation of the Huet–Sayegh model.

$$\boldsymbol{\varepsilon}^* = \frac{1}{E^*(\omega\tau(\theta))}((1+\upsilon)\boldsymbol{\sigma}^* - \upsilon Tr(\boldsymbol{\sigma}^*)\boldsymbol{I}) \tag{3}$$

in which $\boldsymbol{I}$ is the identity tensor. The representation of the Huet–Sayegh model in the Black and Cole–Cole diagrams shows that this model is able to reproduce accurately experimental data stemming from complex modulus tests performed on asphalt materials (Huet, 1963; Sayegh, 1965; Heck et al., 1998).

In ViscoRoute©2.0, the loads are supposed to move at constant speed upon a semi-infinite homogeneous medium, and the problem of quasi-stationary motion is solved in the reference frame ($X = x - Vt$) moving simultaneously with the loads (Frýba, 1999). The solution process is based on a semi-analytical method which consists firstly in solving the problem in the wave number domain after performing a double Fourier transform in the X and y directions. The solution to the original problem (space-time domain) is subsequently obtained by using inverse Fast Fourier Transforms and adequate integration techniques to handle integrable singularities that characterize the solution in the wave number domain (Chupin et al., 2010). The output results of ViscoRoute©2.0 are the mechanical fields (displacement, stress, acceleration, etc.) expressed in any horizontal plane Xy located at a given depth z.

3. Load distribution at the surface of the sub-structure

The load distribution, which links the two sub-systems, is defined assuming that the vertical stress under each sleeper is uniform. According to Vostroukhov and Metrikine (2003), this approximation is valid as far as the waves in the sub-structure are long compared to the spatial dimensions of the sleepers (low-frequency vibrations of the railway track). As explained further in the present study, vertical loads with constant intensity (no impact loading) are used to model a passing train and thus the approximation under discussion is applicable in the frame of continuum modeling. In addition, we assume that the speed of the train is constant and that inertia forces due to the mass of the applied loads can be neglected considering the presence of shock absorbers in vehicles. Under these conditions, the distribution of the vertical stress at the surface of the railway sub-structure can be written under the following generic form:

$$\sigma_{zz}(x,y,z) = [H(y+a) - H(y-a)]\,p(x,t) \tag{4}$$

with

$$p(x,t) = \sum_{n=-\infty}^{n=+\infty}[H(x-nl+b) - H(x-nl-b)]f(nl-Vt) \tag{5}$$

in which n is the sleeper number, $2a$ and $2b$ are the width and the length of the sleepers, l is the center-to-center distance between two sleepers and H is the Heaviside step function. $f(nl - Vt)$ is a master curve that defines the amplitude of the stress distribution and that takes into account the location of the train moving at speed V. The sole function f makes it possible to determine the stress distribution at any time t as shown by Eq. (5) which expresses the fact that $p(x, t + l/V) = p(x - l, t)$ (i.e. points separated by the distance l experience the same pressure history with a delay l/V) if x is the abscissa of a point located under a sleeper and $p(x,t) = 0$ elsewhere, with p uniform under the sleepers. The resulting load exerted by the train being assumed constant and equal to the weight of the train W, f must verify the following condition at any time:

$$\sum_{n=-\infty}^{n=+\infty} f(nl-Vt) = constant = W/(8ab) \tag{6}$$

The space of functions that verifies exactly Eq. (6) is derived in the Appendix A. However, in the present paper, the master curve is not chosen within this function space, but instead a Gaussian-type function is used since it respects Eq. (6) with a good approximation (as shown further) and is easy to handle in the calculations. The computation of f as part of the global solution technique is addressed in Section 7. Prior to that, f is supposed to be known.

As an example, Fig. 3 shows typical distributions (hatched areas) obtained for two different positions of a wheel of a bogie, either right above a sleeper or between two sleepers, and the associated master curve, f. Although the distribution of the vertical stress does not appear the same for the two different positions, the resultant force at the surface of the top layer (sum of the hatched areas in Fig. 3(a) and (b)) is precisely the same in both cases.

4. Decomposition of the loading function or load distribution

To compute the dynamic response of the railway structure based on a quasi-stationary approach, the loading function $p(x,t)$ cannot be directly used such as expressed in Eq. (5). Indeed, such an approach requires the structure under consideration to be homogeneous in the moving direction but also the loading amplitude not to vary with time. To comply with the latter restriction and by using the linearity of the problem, we developed a method based on the decomposition of $p(x,t)$ into functions named "loading waves" that enables us to calculate the dynamic response of the railway structure over a continuous set of moving reference frames. As explained further in this section, the loading waves are continuous functions moving at different speeds, constant with time. The recombination of the loading waves gives the loading function $p(x,t)$.

4.1. The general case for an arbitrary function f

In this section we do not make any assumptions on the definition of the master curve. We start the decomposition by expressing the functions H and f in Eq. (5) as inverse Fourier transforms such that:

$$f(nl-Vt) = \frac{1}{2\pi}\int_{-\infty}^{\infty}\hat{f}(q)\,e^{iq(nl-Vt)}dq \tag{7}$$

and,

$$H(x) = \frac{1}{2i\pi}PV\int_{-\infty}^{\infty}\frac{e^{ipx}}{p}dp + \frac{1}{2} \tag{8}$$

in which $\hat{f}$ is the Fourier transform of the master curve and i the imaginary unit. PV denotes the principal value of the integral.

Using the distribution theory and substituting Eqs. (7) and (8) into Eq. (5) lead to:

$$p(x,t) = \frac{1}{4i\pi^2}\sum_{n=-\infty}^{n=+\infty}\left(\int_{-\infty}^{+\infty}\frac{e^{ip(x-nl+b)} - e^{ip(x-nl-b)}}{p}dp\int_{-\infty}^{+\infty}\hat{f}(q)\,e^{iq(nl-Vt)}dq\right) \tag{9}$$

or equivalently,

$$\begin{aligned} p(x,t) &= \frac{1}{4i\pi^2}\int_{-\infty}^{+\infty}\int_{-\infty}^{+\infty}\hat{f}(q)\frac{e^{i(px+pb-qVt)} - e^{i(px-pb-qVt)}}{p}\sum_{n=-\infty}^{n=+\infty}e^{-in(p-q)l}dpdq \\ &= \frac{1}{4i\pi^2 l}\int_{-\infty}^{+\infty}\int_{-\infty}^{+\infty}\hat{f}\left(\frac{q}{l}\right)\frac{e^{i(px+pb-qVt)/l} - e^{i(px-pb-qVt)/l}}{p}\sum_{n=-\infty}^{n=+\infty}e^{-in(p-q)}dpdq \end{aligned} \tag{10}$$

The following relation for the infinite sum of the exponential function can be deduced: $\sum_{n=-\infty}^{n=+\infty}e^{-inr} = 2\pi\sum_{n=-\infty}^{n=+\infty}\delta(r-2n\pi)$, δ being the Dirac delta function. Then, Eq. (10) can be rewritten as follows:

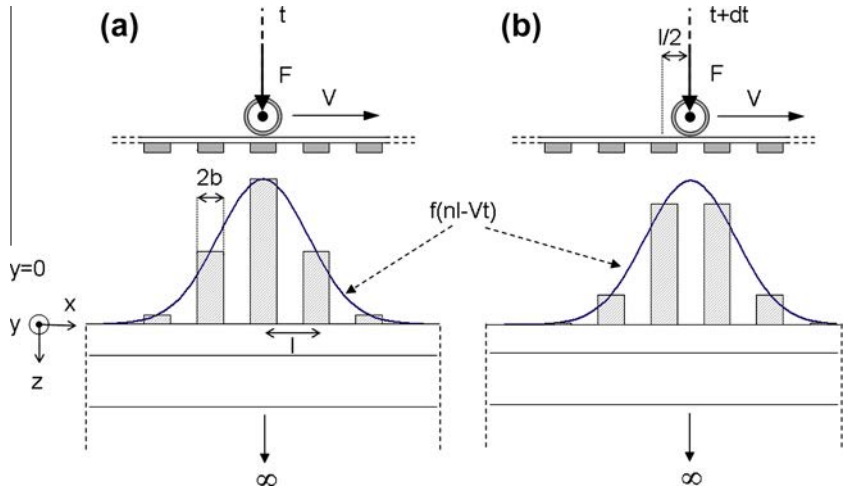

Fig. 3. Master curve and distribution of vertical stress (hatched areas) at the surface of the topmost layer of the railway structure excited by one wheel of a bogie. (a) The load is located right above a sleeper; (b) the load is located between two sleepers.

$$p(x,t)=\frac{1}{4i\pi^2 l}\int_{-\infty}^{+\infty}\int_{-\infty}^{+\infty}\hat{f}\left(\frac{q}{l}\right)\frac{e^{ip\left(x+b-\frac{qV}{p}t\right)/l}-e^{ip\left(x-b-\frac{qV}{p}t\right)/l}}{p}\times\left[2\pi\sum_{n=-\infty}^{n=+\infty}\delta(p-q-2n\pi)\right]dpdq \tag{11}$$

and after integration with respect to p:

$$p(x,t)=\frac{1}{2i\pi l}\sum_{n=-\infty}^{n=+\infty}\int_{-\infty}^{+\infty}\hat{f}\left(\frac{q}{l}\right)\frac{e^{i(2n\pi+q)\left(x+b-\frac{qV}{2n\pi+q}t\right)/l}-e^{i(2n\pi+q)\left(x-b-\frac{qV}{2n\pi+q}t\right)/l}}{2n\pi+q}dq \tag{12}$$

Note that now Eq. (12) makes sense in the usual way of summation and integration provided that $\hat{f}$ is conveniently chosen (see further for the choice of a Gaussian type function).

Let us now make the following change of variable:

$$v=\frac{qV}{2n\pi+q} \tag{13}$$

which in turn leads to:

$$q=2n\pi\frac{v}{V-v}\ \text{and}\ dq=2n\pi\frac{V}{(V-v)^2}dv\ \text{or}\ \frac{dq}{2n\pi+q}=\frac{dv}{V-v} \tag{14}$$

As a consequence of Eq. (14), if n is positive, the variable v varies from V to $+\infty$ when $-\infty<q<-2n\pi$ and from $-\infty$ to V when $-2n\pi<q<+\infty$. On the other hand, if n is negative, v varies from V to $-\infty$ when $-\infty<q<-2n\pi$ and from $+\infty$ to V when $-2n\pi<q<+\infty$. The above change of variable applied to Eq. (12) gives:

$$p(x,t)=\frac{1}{2i\pi l}\int_{-\infty}^{+\infty}\frac{1}{V-v}\times\left[\begin{array}{l}\sum_{n=1}^{\infty}\hat{f}\left(2n\pi\frac{1}{l}\frac{v}{V-v}\right)\left(e^{i2n\pi\frac{V}{V-v}\frac{(x+b-vt)}{l}}-e^{i2n\pi\frac{V}{V-v}\frac{(x-b-vt)}{l}}\right)\\-\sum_{n=-1}^{-\infty}\hat{f}\left(2n\pi\frac{1}{l}\frac{v}{V-v}\right)\left(e^{i2n\pi\frac{V}{V-v}\frac{(x+b-vt)}{l}}-e^{i2n\pi\frac{V}{V-v}\frac{(x-b-vt)}{l}}\right)\end{array}\right]dv+\frac{1}{2i\pi l}\int_{-\infty}^{+\infty}\hat{f}\left(\frac{q}{l}\right)\frac{e^{iq(x+b-Vt)/l}-e^{iq(x-b-Vt)/l}}{q}dq \tag{15}$$

By setting $v=\alpha V$ and by switching, for any real value of α, to the moving basis defined by ${}^{\alpha}X=x-\alpha Vt$ and ${}^{1}X$ for $\alpha=1$, Eq. (15) becomes:

$$p(x,t)=\int_{-\infty}^{+\infty}g(x-\alpha Vt,\alpha)\,d\alpha+\frac{1}{l}\int_{x-Vt-b}^{x-Vt+b}f(x)\,dx=\int_{-\infty}^{+\infty}g({}^{\alpha}X,\alpha)\,d\alpha+\frac{1}{l}\int_{{}^{1}X-b}^{{}^{1}X+b}f(x)\,dx \tag{16}$$

with, for $\alpha\neq 1$,

$$g({}^{\alpha}X,\alpha)=\frac{1}{2i\pi l}\frac{1}{1-\alpha}\sum_{n=1}^{\infty}\left[\begin{array}{l}\hat{f}\left(n\frac{2\pi}{l}\frac{\alpha}{1-\alpha}\right)e^{in\frac{2\pi}{1-\alpha}\frac{{}^{\alpha}X+b}{l}}-\hat{f}\left(-n\frac{2\pi}{l}\frac{\alpha}{1-\alpha}\right)e^{-in\frac{2\pi}{1-\alpha}\frac{{}^{\alpha}X+b}{l}}\\-\hat{f}\left(n\frac{2\pi}{l}\frac{\alpha}{1-\alpha}\right)e^{in\frac{2\pi}{1-\alpha}\frac{{}^{\alpha}X-b}{l}}+\hat{f}\left(-n\frac{2\pi}{l}\frac{\alpha}{1-\alpha}\right)e^{-in\frac{2\pi}{1-\alpha}\frac{{}^{\alpha}X-b}{l}}\end{array}\right] \tag{17}$$

Eq. (16) reflects the fact that $p(x,t)$ can be in part expressed as the superimposition of the loading waves $g({}^{\alpha}X,\alpha)=g(x-\alpha Vt,\alpha)$ moving at positive or negative speed $v=\alpha V$ (α varying from $-\infty$ to $+\infty$). The second term in the right hand side of Eq. (16) represents the contribution of a specific wave moving at speed V ($\alpha=1$) and having the shape of f. Note that the wave function g is periodic with X^{α} of period $(1-\alpha)l$. Moreover, for a real symmetric function $f(x)$ (as it will be encountered further in this article), the Fourier transform is a real function and verifies $\hat{f}(q)=\hat{f}(-q)$. Then, for $\alpha\neq 1$, Eq. (17) becomes:

$$g({}^{\alpha}X,\alpha)=\frac{1}{\pi l}\frac{1}{1-\alpha}\sum_{n=1}^{\infty}\hat{f}\left(n\frac{2\pi}{l}\frac{\alpha}{1-\alpha}\right)\times\left[\sin\left(n\frac{2\pi}{1-\alpha}\frac{{}^{\alpha}X+b}{l}\right)-\sin\left(n\frac{2\pi}{1-\alpha}\frac{{}^{\alpha}X-b}{l}\right)\right] \tag{18}$$

Then, under the assumptions of the present study, in particular the linearity of the constitutive laws, the response of the sub-structure to a train moving at constant speed can be obtained by superimposing the responses of the sub-structure to each loading wave defined by Eq. (18) plus the one corresponding to the second term of the right hand side of Eq. (16) (loading wave moving at speed V). In what follows, the response to a given loading wave characterized by a given value of α in Eq. (18) is computed using ViscoRoute©2.0 numerical program (see Section 2.2).

Note: it can be shown that in the right hand side of Eq. (16) the integral with respect to x of the term associated to the wave moving at speed V ($a=1$) is equal to the integral of $p(x,t)$, which is itself equal to $W/4a$ that is the weight of the train (or bogie) divided by the width ($4a=2\times 2a$) of the sleepers for the two rails. Numerical applications show that this loading wave is dominant in the computation of acceleration and thus can be used standalone as an

external load applied on the sub-structure to obtain a first approximate of the acceleration field (calculation avoiding the modeling of rails and sleepers). Nonetheless, the computation of other mechanical fields such as stress requires the consideration of a wider spectrum of loading waves of type $g({}^{\alpha}X, \alpha)$ (Chupin and Piau, 2011).

4.2. Loading decomposition for a Gaussian-type master curve

The master curve must be taken in a specific function space to ensure the condition of Eq. (6). However, as mentioned earlier, a Gaussian-type function which does not lie within this space of functions allows Eq. (6) to be approached with a reasonable accuracy, provided that it has a width sufficiently large compared to the distance between two sleepers. Moreover, as it is shown further in the numerical example, the Gaussian-type function fits well the distribution of the vertical stress at the surface of the layered structure. For these reasons and also for an easy use in the numerical calculations, the master curve is chosen as the sum of Gaussian functions:

$$f(x) = \sum_{i=1}^{nloads} A_i e^{-\left(x - x^i_{axle}\right)^2 / L_i^2} \tag{19}$$

in which *nloads* is the number of wheels applied on the rails and x^i_{axle} is the location of axle *i*. The Gaussian-type function is characterized by the parameters A_i and L_i. Now, Eq. (18) that defines the amplitude of the loading waves can be evaluated for the Gaussian-type function defined above, whose Fourier transform in the case of one load with $x^1_{axle} = 0$ is:

$$\hat{f}(q) = A\sqrt{\pi} L e^{-L^2 q^2/4} \tag{20}$$

Then, Eq. (18) becomes:

$$g({}^{\alpha}X, \alpha) = \frac{A}{\sqrt{\pi}} \frac{L}{l} \frac{1}{1-\alpha} \sum_{n=1}^{\infty} e^{-\left(n \frac{\pi L}{l} \frac{\alpha}{1-\alpha}\right)^2} \times \left[\sin\left(n \frac{2\pi}{1-\alpha} \frac{{}^{\alpha}X + b}{l}\right) - \sin\left(n \frac{2\pi}{1-\alpha} \frac{{}^{\alpha}X - b}{l}\right)\right] \tag{21}$$

Note that for α in the vicinity of 1, the function *g* is well-defined since $\lim_{\alpha \to 1} g({}^{\alpha}X, \alpha) = 0$ and that the Gaussian function effectively leads to a finite value of the sum in Eq. (21).

As an illustration of the decomposition method, Fig. 4 shows some of the loading waves obtained by considering the parameters of the numerical example (Section 8) and for a master curve defined according to the Gaussian-like function. The recombination of the loading is also illustrated in the numerical example.

5. Numerical treatment of the decomposition method

In this section, we explain how the decomposition method is implemented in a numerical code for computing the dynamic response of the sub-structure to a passing train.

We have shown in Section 3 that the load applied at the surface of the structure could be decomposed into loading waves moving at different speeds. The interesting point is that, unlike the stress distribution defined by Eq. (5), each of the loading waves can be formulated independently of time (in its own moving reference frame) and thus can be used as an input for the quasi-stationary calculation of the dynamic response of the sub-structure with ViscoRoute©2.0. The response of the sub-structure to the actual loading induced by a passing train is then obtained by recombining the responses due to every loading wave.

In order to compute the dynamic response of the railway sub-structure using a numerical approximation, the first integral of the right hand side in Eq. (16) is evaluated through the discretization of the integration variable α. The integration range that extends from $-\infty$ to $+\infty$ is reduced to a finite interval $I_\alpha = [\alpha_1, \alpha_{N+1}]$ which is discretized into *N* subintervals of equal length $\Delta\alpha$. The integration is performed by applying a trapezoidal rule on each of them. On the other hand, the second integral of the right hand side of Eq. (16) is simply calculated using a midpoint approximation that yields:

$$\frac{1}{l} \int_{{}^{1}X-b}^{{}^{1}X+b} f(x)\, dx \approx f({}^{1}X) \frac{2b}{l} \tag{22}$$

Finally, the stress distribution can be approached by the following discretized form:

$$p(x,t) \approx \Delta\alpha \left[\frac{g({}^{\alpha_1}X, \alpha_1) + g({}^{\alpha_N}X, \alpha_N)}{2} + \sum_{\alpha_2}^{\alpha_{N-1}} g({}^{\alpha_i}X, \alpha_i)\right] + f({}^{1}X) \frac{2b}{l} \tag{23}$$

Using Eq. (23), the dynamic response of the sub-structure is computed for "wave packets" localized in α_i and resulting from the sum of the loading waves taken within an interval $\Delta\alpha$ around this point. The response of the sub-structure to the global loading is obtained by summing the dynamic responses due to each individual "wave packet" and the particular wave moving at speed *V* (corresponding to second term of the right hand side of Eq. (23)). The length of I_α and the number of subintervals are chosen such that they give an accurate representation of the stress distribution at the surface of the railway sub-structure once the recombination of the loading has been performed by summation of the contribution of every discretized loading wave.

Using the decomposition of Eq. (23), the dynamic response of the sub-structure to every loading wave is computed using the numerical program ViscoRoute©2.0. In the latter, the load is represented by a set of elliptical- or rectangular-shaped areas, on each of which a uniform pressure distribution is applied. Consequently, to respect the representation of the input loading in ViscoRoute©2.0 and prior to compute the mechanical response to a given loading wave (input for ViscoRoute©2.0), the latter is discretized in *X* (discretization points denoted ${}^{\alpha_i}X_j$) and a uniform pressure $P_0({}^{\alpha_i}X_j)$ is applied on each interval of length dX_{α_i} centered in ${}^{\alpha_i}X_j$. In order to keep the discrete value of the integral of that loading wave (resultant force) equal to the analytical value, $P_0({}^{\alpha_i}X_j)$ can be advantageously computed such as:

$$P_0\left({}^{\alpha_i}X_j\right) = \frac{G\left({}^{\alpha_i}X_j + \frac{dX_{\alpha_i}}{2}\right) - G\left({}^{\alpha_i}X_j - \frac{dX_{\alpha_i}}{2}\right)}{dX_{\alpha_i}} \tag{24}$$

in which *G* is the integral of *g* with respect to ${}^{\alpha}X$, provided that *G* has an analytical expression.

In the case of the master curve being defined by a Gaussian-type function, *g* is given by Eq. (21) and its integral reads ($\alpha \neq 1$):

$$G({}^{\alpha}X, \alpha) = \frac{AL}{2\pi^{3/2}} \sum_{n=1}^{n=+\infty} \frac{e^{-\left(n \frac{\pi L}{l} \frac{\alpha}{1-\alpha}\right)^2}}{n} \times \left[-\cos\left(n \frac{2\pi}{1-\alpha} \frac{{}^{\alpha}X + b}{l}\right) + \cos\left(n \frac{2\pi}{1-\alpha} \frac{{}^{\alpha}X - b}{l}\right)\right] \tag{25}$$

To get the discretized loading owing to "wave packet" α_i, Eq. (25) is evaluated at points ${}^{\alpha_i}X_j \pm dX_{\alpha_i}/2$, and substituted into Eq. (24). This must be done for all the points, ${}^{\alpha_i}X_j$. Practically, since $G({}^{\alpha}X, \alpha)$ is a periodic function in ${}^{\alpha}X$, the loading due to "wave packet" α_i is considered over one period defined by $l(1 - \alpha_i)$, i.e. ${}^{\alpha}X_j$ are chosen within this period interval, and the response to the complete signal that characterizes the "wave packet" α_i is obtained using the superposition principle for a large number of periods so that the corresponding loading extends far from the region where the mechanical fields need to be evaluated.

After running ViscoRoute©2.0 for all the "wave packets", the dynamic response of the structure is visualized at points of a

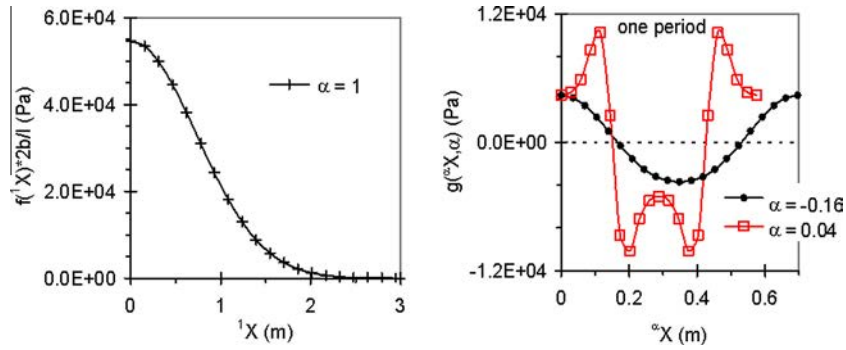

Fig. 4. Example of loading waves (amplitude).

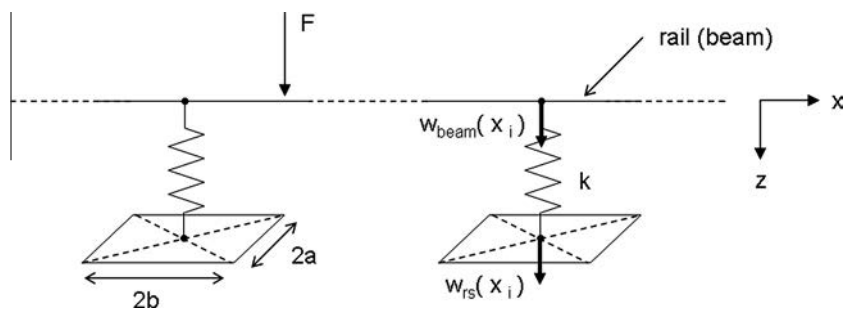

Fig. 5. Schematic representation of the rail/sleeper system.

projection grid (x,y,z) which is set in the fixed reference frame tied to the railway structure. Then, the recombination of the loading and of any mechanical field, $c(x,y,z,t)$, computed by ViscoRoute©2.0 is obtained by the summation:

$$c(x,y,z,t) = \sum_{\alpha 1}^{\alpha_N} c_{\alpha_i}({}^{\alpha_i}X,y,z) + c_1({}^1X,y,z) \tag{26}$$

Given the FFT algorithm used in ViscoRoute©2.0, the sampling theorem (Shannon, 1949) can be utilized to interpolate field c_{α_i} at the x locations of the grid using the relationship:

$${}^{\alpha_i}X = x - \alpha_i Vt.$$

To summarize, a numerical code with successive calls to ViscoRoute©2.0 was developed to implement the different steps above (denoted "loop on α" in Fig. 6), as well as the calculation of the master curve explained in the next section (see Fig. 6 for the global iterative process). In practice, the mechanical fields of interest are determined by running an additional "loop on α" after the iterative process in Fig. 6 has converged, i.e. once the master curve is known. After running the numerical simulations, a post-processing vs. space and time is performed. This numerical approach was validated on a case study by comparison to finite element simulations in the case of low speeds. One advantage of the developed method is that it takes only a few minutes to compute the dynamic response of the railway structure to a moving load. This will be of great interest in the parametric studies.

In particular, these computations ("loop on α") make it possible to compute w_{rs}^i, the displacements under the sleepers, to a given set of pressure values, p_s^i. In what follows, the resultant forces under the sleepers $F_s^i = 4ab \times p_s^i$ are used instead of p_s^i.

6. Modeling of the track/sleeper system

As shown in Fig. 5, the track/sleeper system is modeled by Euler–Bernoulli beams resting on vertical springs. The degrees of freedom (DOF) considered for this system are the vertical displacement and the slope of the beam (resp. w_{beam} and θ_{beam}) and the deflection (w_{rs}) of the sub-structure.

The equilibrium equations of the track/sleeper system are first derived by assuming a displacement field of the sub-structure, w_{rs}^i, considering that the stiffness, k, is the same for all the springs. The vertical force F_i^s exerted by a given spring on the trackbed is defined by:

$$F_i^s = k(w_{beam}(x_i) - w_{rs}(x_i)) \tag{27}$$

in which x_i is the point of application of the force located at the center of sleeper i. In accordance, the equilibrium equation for a bending beam resting on m (possibly $+\infty$) springs and excited by a vertical force F applied at location x_F is:

$$EI\frac{d^4 w_{beam}(x)}{dx^4} + \sum_{i=1}^{m} k[w_{beam}(x_i) - w_{rs}(x_i)]\,\delta(x - x_i) = F\,\delta(x - x_F) \tag{28}$$

E and I are the elastic modulus and the second moment of inertia of the beam. δ is the Dirac delta function. The DOF at the end nodes of the beam are considered free of external forces. It is checked *a posteriori* that their values are negligible as expected far from the load location.

Assuming an elastic behavior of the typical element made up of a portion of the beam resting on a spring at each of its ends, the characteristic relationship in matrix form between the forces acting on the nodes $\{F\}^e$ and the nodal displacements $\{w_b\}^e$ reads (Zienkiewicz, 1971):

$$\{\boldsymbol{F}\}^e = [\boldsymbol{K}]^e\{\boldsymbol{w}_b\}^e + \{\boldsymbol{F}\}_p^e \tag{29}$$

in which $\{\boldsymbol{F}\}_p^e$ represents the nodal forces required to balance any loads (distributed or point force) acting on the element. $\{\boldsymbol{F}\}_p^e$ can be easily derived using for example the Maxwell–Betti reciprocal work theorem (see also Hammoud et al., 2010). For the case of a

given K_{bb}, K_{bs} and F_b
$w_{rs}^0 = 0$; $i = 0$
do {
$i \leftarrow i + 1$
$w_b^i \leftarrow K_{bb}^{-1}\left[F_b - K_{bs} w_{rs}^{i-1}\right]$
$F_s^i \leftarrow k\left(w_b^i - w_{rs}^{i-1}\right)$
fitting of $F_s^i/4ab \rightarrow f^i(x)$

decomposition of the loading $\rightarrow$ $g^i\left({}^{\alpha}X, \alpha\right)$
computation of $w_{rs,\alpha}^i$ for each $g^i\left({}^{\alpha}X, \alpha\right)$ and $f\left({}^{1}X\right)\frac{2b}{l}$
recombination : $w_{rs}^i \leftarrow \sum_{\alpha} w_{rs,\alpha}^i\left({}^{\alpha}X\right) + w_{rs,1}^i\left({}^{1}X\right)$
} loop on α

} while $\{max\left(\left|w_{rs}^i - w_{rs}^{i-1}\right|\right) > \epsilon\}$
$f(x) \leftarrow f^i(x)$
computation of the dynamic response : loop on α

Fig. 6. Schematic algorithm used for the computation of the master curve and the dynamic response of the railway structure.

point force applied at distance d from the left end of the typical element, it reads:

$$\{\boldsymbol{F}\}_p^e = F\begin{bmatrix} \frac{-2d^3+3d^2l-l^3}{l^3} \\ \frac{-d^3+2d^2l-dl^2}{l^2} \\ \frac{2d^3-3d^2l}{l^3} \\ \frac{-d^3+d^2l}{l^2} \end{bmatrix} \tag{30}$$

in which l is the element length (center to center distance between two sleepers). In Eq. (29), $[\boldsymbol{K}]^e$ is the element stiffness matrix which, for a current typical element, reads:

$$[\boldsymbol{K}]^e = EI\begin{bmatrix} \frac{12}{l^3}+\frac{k}{2EI} & \frac{6}{l^2} & \frac{-12}{l^3} & \frac{6}{l^2} \\ \frac{6}{l^2} & \frac{4}{l} & -\frac{6}{l^2} & \frac{2}{l} \\ \frac{-12}{l^3} & -\frac{6}{l^2} & \frac{12}{l^3}+\frac{k}{2EI} & -\frac{6}{l^2} \\ \frac{6}{l^2} & \frac{2}{l} & -\frac{6}{l^2} & \frac{4}{l} \end{bmatrix} \tag{31}$$

The displacement $\{\boldsymbol{w}_b\}^e$ related to Eq. (31) is: $\{\boldsymbol{w}_b\}^e = [\,w_{beam}(x_k) \quad \theta_{beam}(x_k) \quad w_{beam}(x_{k+1}) \quad \theta_{beam}(x_{k+1})\,]$, with the classical expression of the slope of the beam, $\theta_{beam} = dw_{beam}/dx$.

The global system is composed of $m-1$ typical elements and the equilibrium equation must be satisfied at all the nodes of these elements. To derive the equilibrium equation at a typical node k, each quantity involved in the equilibrium has to be equated to the sum of the individual contributions brought by the elements meeting at this node. Therefore this summation concerns only the elements which contributes to node k. This procedure is repeated for all nodes and the structural problem is defined by assembling the equilibrium equations derived at each node. The following discrete equation is then obtained:

$$[\boldsymbol{K}_{bb} \quad \boldsymbol{K}_{bs}]\begin{Bmatrix} \boldsymbol{w}_b \\ \boldsymbol{w}_{rs} \end{Bmatrix} = \{\boldsymbol{F}_b\} \tag{32}$$

with $\boldsymbol{K}_{bb} = \sum[\boldsymbol{K}]^e$ and $\{\boldsymbol{F}_b\} = \sum(\{\boldsymbol{F}\}^e - \{\boldsymbol{F}\}_p^e)$ in which the element contributions have been evaluated according to the aforementioned prescriptions. In Eq. (32), the components of $\boldsymbol{K}_{bs}$ are defined as follows:

$$K_{bs}^{pq} = k\delta(p-2q+1), \quad p = \{1,\ldots,2m\}, \quad q = \{1,\ldots,m\} \tag{33}$$

The nodal displacements and forces of Eq. (32) reads:

$$\boldsymbol{w}_b = \{\,w_{beam}^1 \quad \theta_{beam}^1 \quad \cdots \quad w_{beam}^m \quad \theta_{beam}^m\,\}^T, \quad \boldsymbol{F}_b = \{\,F_b^1 \quad \cdots \quad F_b^{2m}\,\}^T,$$
$$\boldsymbol{w}_{rs} = \{\,w_{rs}^1 \quad \cdots \quad w_{rs}^m\,\}^T \tag{34}$$

7. Coupling between the track/sleeper system and the sub-structure and iterative calculation of the master curve parameters

The coupling between the track/sleeper system and the sub-structure is performed using a fixpoint iterative procedure based on the determination of arrays $\boldsymbol{w}_{rs}$ and $\boldsymbol{F}_s$. The solution algorithm is given in Fig. 6. To summarize, it consists in searching $\boldsymbol{F}_s$ at iteration i (superscript i in the expressions of Fig. 6 denotes the iteration index), $\boldsymbol{w}_{rs}$ being known at the preceding iteration $i-1$ ($\boldsymbol{w}_{rs}$ is initialized to zero). The forces in the springs are deduced from $\boldsymbol{w}_b^i$, $\boldsymbol{w}_{rs}^{i-1}$ and the stiffness k of the springs. They are then expressed in terms of vertical stress applied at the surface of the sub-structure and fitted by a sum of Gaussian-type functions (simple iterative procedure that consists in minimizing the square difference between the sum of the Gaussian-type functions and the computed forces in the springs) to produce the master curve at iteration i, $f^i(x)$. At that point, the decomposition method described in Section 3 is applied with $f^i(x)$ in order to compute the deflection (inertia effects included) of the railway structure at iteration i, $\boldsymbol{w}_{rs}^i$. In Fig. 6, this step is denoted "loop on α" within which $\boldsymbol{w}_{rs,\alpha}^i$ represents the deflection due to "wave packet" α at iteration i. The iterations are stopped when w_{rs} (or equivalently $\boldsymbol{w}_b$) does not vary more than a small positive quantity ε over the iterations. Numerically, this is reflected by the following criterion:

$$\max(|\boldsymbol{w}_{rs}^i - \boldsymbol{w}_{rs}^{i-1}|) < \varepsilon \tag{35}$$

Once Eq. (35) is verified, the master curve with inertial forces in the sub-structure is set equal to $f^i(x)$ computed at the last iteration.

In the next section, the iterative procedure is validated by comparison to FE simulations performed at low speeds for a sub-structure composed of elastic layers only. Let us note that very few iterations are needed to converge to the master curve.

8. Numerical example and validation of the implemented method

In this section, we use the developed method to compute the dynamic response of a railway structure subjected to the bogie of a high-speed train driven at constant speed. The simplified sub-structure considered herein (Fig. 7) is defined such that it is roughly representative of a real railway structure. Nonetheless, the purpose of this section is to validate and to better apprehend the developed method rather than to conduct a case study. The structure is composed of three layers. The topmost layer could represent a ballast layer and is assumed to be linear elastic. For the purpose of illustration, the sub-ballast layer is considered either linear elastic or viscoelastic to represent in the latter case a layer of asphalt paving material. The rails and the sleepers laid on this structure (not represented in Fig. 7) are modeled by Euler–Bernoulli beams (steel beams of characteristics: $E_{beam} = 210$ GPa and $I_{beam} = 3 \times 10^{-5}$ m^4) and springs of stiffness 5×10^7 N/m, respectively. The considered loading applied on the rails is a bogie with four wheels (see Fig. 1), each wheel being represented by a point force of 80 kN acting in the vertical direction. The distance between the two axles of the bogie is $db = 3$ m and the distance between the rails is set to $dr = 1.5$ m.

8.1. Case of a linear elastic underlayer

The validation of the developed method is performed by comparison with finite element (FE) simulations for a whole railway composed of elastic layers. The FE simulations are performed with the software CESAR–LCPC which is an in-house developed code that includes standard functionalities of FEM. The FE simulations

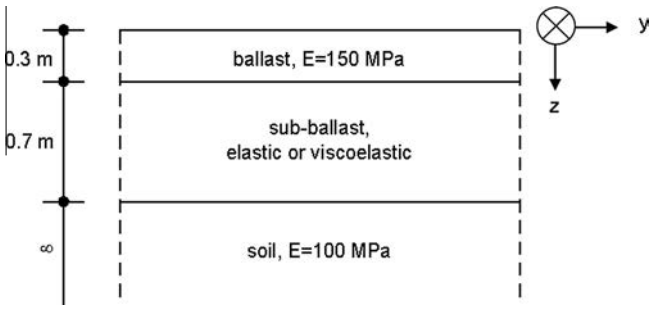

Fig. 7. Schematic representation of a vertical section of the structure under study.

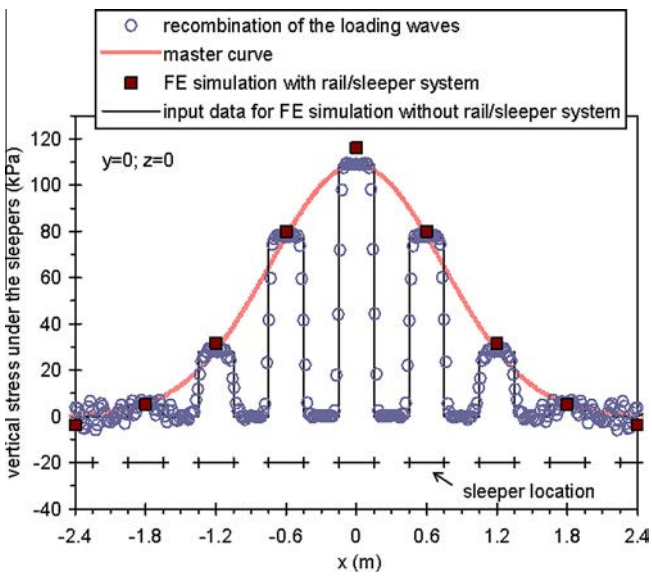

Fig. 8. Comparison between the recombination of the loading waves (and master curve) obtained from the semi-analytical method and the vertical stress distribution under the sleepers arising from FE simulations ($E_{plate} = 1.75 \times 10^7$ MPa) for one wheel of the bogie located in $x = 0$.

are run without taking into account the inertia effects in the structure. As shown further in this section, at relatively low speeds of the moving loads, such FE simulations are nonetheless in good agreement with the developed semi-analytical method that solves the full dynamic problem.

In the FE simulations, the rails are modeled by volume elements and their section is assumed to be rectangular with a moment of inertia equal to I_{beam}. The rails are tied to the structure through elements (SPR) of special rigidity that make it possible to enforce the mechanical connection between the rails and the trackbed to be the same as the one used in the developed method and modeled by springs of rigidity k. The SPR elements are laid on thin rigid plates (of dimensions $2a \times 2b = 0.3 \times 0.8$ m^2 and of Young's modulus E_{plate}) that distribute the vertical load at the surface of the railway structure.

The structure under consideration is the one in Fig. 7 for which the sub-ballast is assumed linear elastic with Young's modulus equal to 120 MPa. The Young modulus of the topmost layer is chosen such that no traction stress develops in this layer which is supposed to represent a non-cohesive granular material. Additionally, it is assumed that all the layers have the same density equal to 1800 kg/m^3. The mechanical response of this structure is computed using both the semi-analytical method and FE simulations. In the developed method, Eq. (16) that gives the stress distribution under the sleepers is computed numerically using the following discretization: $I_\alpha = [-0.8, 0.8] \cup \{\alpha = 1\}$ and $N = 40$, i.e. 40 loading waves are use to evaluate the integral with respect to α in Eq. (16).

8.1.1. Validation of the developed method

When a train bogie is driven at low speed on the rails, the inertia effects in the structure are quite negligible. This makes it possible for us to validate the developed method and in particular the decomposition/recombination technique as well as the computation of the master curve (through the association of discrete and continuum models) by comparison with the aforementioned FE simulations. Consequently, a relatively low speed equal to 50 m/s is chosen in this section. Then, the developed method is compared to FE simulations in terms of stress distribution, σ_{zz}, under the sleepers and deflection, u_z. These quantities are plotted in Figs. 8 and 9 for a given time t corresponding to the wheels of the bogie positioned right above the sleeper centers. With regards to the stress distribution, we look at the horizontal profile in the x-direction plotted for $z = 0$ (surface of the trackbed) and $y = 0$ (under a rail axis). The master curve after convergence computed for the present example is shown in Fig. 8 (thick continuous line) for one wheel of the bogie. It is a Gaussian function whose parameters are equal approximately to: $A \approx 115$ kPa and $l \approx 1$ m. The recombination of the 40 loading waves stemming from the master curve is displayed with circle symbols in Fig. 8. At the sleeper centers, σ_{zz} obtained from the recombination is superimposed on the master curve. It clearly appears that the stress distribution arising from the recombination reproduces accurately the actual shape of σ_{zz} that exhibits non-zero values only under the sleepers.

Moreover, the amplitude of σ_{zz} obtained by recombination of the loading waves is in good agreement with the FE simulation displayed in Fig. 8. The FE simulation is performed for the global railway including the rail/sleeper system (black filled square symbols) for which σ_{zz} is plotted at the sleeper centers (i.e. far from the edges of the rigid plates where stress singularities are present). Fig. 8 shows also the external loading (thin black line) for another FE simulation which was performed by replacing the rail/sleeper system at the surface of the trackbed by a step distribution of uniform pressures defined from the master curve. The result of this simulation is presented in Fig. 9 in terms of deflection.

Fig. 9 shows the horizontal profile of u_z in the x-direction plotted for $z = 0.05$ m and $y = 0$ (under a rail axis). The deflection obtained with the developed method compares well with the FE simulations run with and without the rail/sleeper system. It can be noticed also that the primary and secondary peaks of u_z are obtained under the sleepers located in the vicinity of the position of the wheels ($x = 0$ and $x = 3$ m).

It can be shown that the good agreement between the developed method and the FE simulations extends also to other fields (see for example the results on the vertical acceleration shown in the next section).

8.1.2. Influence of dynamic effects at high speeds

The role of the dynamic effects is now highlighted by running the developed method for a higher speed ($V = 95$ m/s) and by comparing the computed vertical acceleration, γ_z, to the one obtained using FE simulations without inertia forces. In the latter case, γ_z is computed from the second derivative with respect to time of the deflection u_z (post-treatment), u_z being reconstructed from several static computations performed for different positions of the bogie.

The time evolution of γ_z is plotted in Fig. 10 for a particular point located under a sleeper center at a depth of 0.05 m (top of the ballast layer). The peaks of upward γ_z observed in this figure correspond to an axle of the bogie driven right above the point of observation (at $t = 0$ the rear axle is passing above this point). At $V = 50$ m/s the difference between the calculations performed with

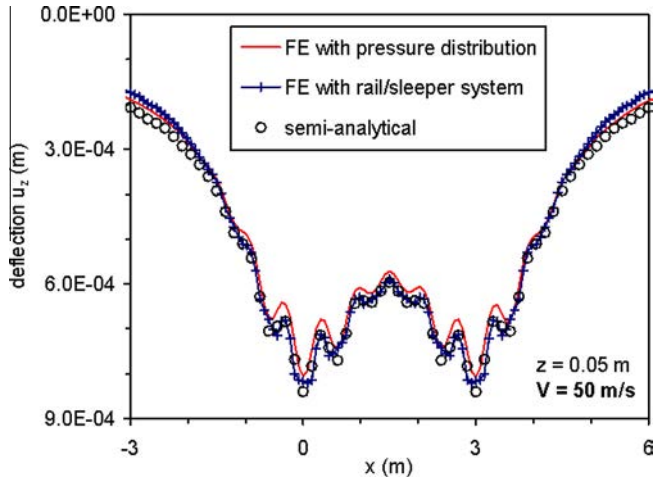

Fig. 9. Profile in the x-direction of the deflection in $z = 0.05$ m computed at a given time t corresponding to the wheels of the bogie positioned right above sleeper centers in $x = 0$ and $x = 3$ m.

and without inertia forces is negligible as attested by the superimposition of the curves in this case (this result is in accordance to what was shown in Section 8.1.1). Nevertheless, at $V = 95$ m/s inertia forces in the structure impact the calculation of γ_z and, at this speed, an amplification of the vertical acceleration around 15–20% is noticeable at the extrema of the curves when they are computed with inertia forces. So at high speeds, inertia effects in the trackbed start being significant. Note also that at $V = 95$ m/s the peak values of γ_z are about 4 times greater than at $V = 50$ m/s.

8.2. Case of a linear viscoelastic underlayer

To further illustrate the potential of the developed method we consider in this section a structure that incorporates a layer of asphalt paving material (underlayer).

Note that in this case, static computations as those used in the FE simulations of Section 8.1 cannot be done since in viscoelasticity the response of the material depends on the speed. The structure under consideration is that of Fig. 7 for which the sub-ballast layer is assumed to be linear viscoelastic according to the Huet–Sayegh model whose parameters are given in Table 1. A bogie is driven on this structure at a speed of 95 m/s and γ_z is computed for two temperatures of the asphalt layer equal to $T = 15$ °C and $T = 45$ °C. The parameters of the master curves obtained at these different

Table 1
Value of the Huet Sayegh parameters.

E_∞ (MPa)	E_0 (MPa)	δ	h	k	A_0	A_1	A_2
32665	110	2.24	0.59	0.19	2.94	−0.40	1.95E−3

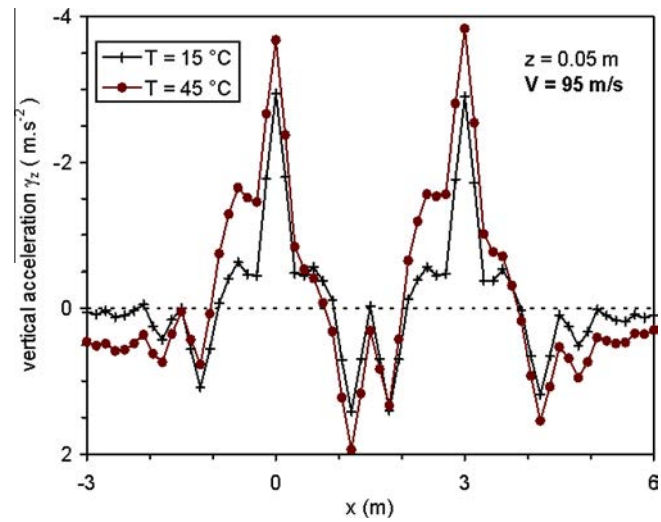

Fig. 11. Horizontal profile of the vertical acceleration in the ballast layer and under a rail axis ($y = 0$, $z = 0.05$ m): influence of temperature.

temperatures are almost the same with a value of $A \approx 120$ kPa and $l \approx 0.97$ m (close to the values obtained for the elastic structure). The horizontal profile of γ_z (in $y = 0$ and $z = 0.05$ m, i.e. in the ballast layer) computed with the developed method is shown in Fig. 11 for the two tested temperatures and for a given time t corresponding to the wheels of the bogie located in $x = 0$ and $x = 3$ m.

In both downward and upward directions, the peak values of γ_z in $z = 0.05$ m are higher at $T = 45$ °C than at $T = 15$ °C, i.e. as the asphalt layer positioned under the topmost layer becomes softer. Indeed asphalt materials are thermo-sensitive and their stiffness decreases with temperature. We also notice that, due to the viscoelastic behavior of the underlayer, the symmetry of the response is lost at $T = 45$ °C. By comparison with the results shown in Fig. 10 ($V = 95$ m/s) we finally note that the amplitude of γ_z is divided by more than 2 for the structure incorporating the asphalt layer because of a higher stiffness of the underlayer in this case.

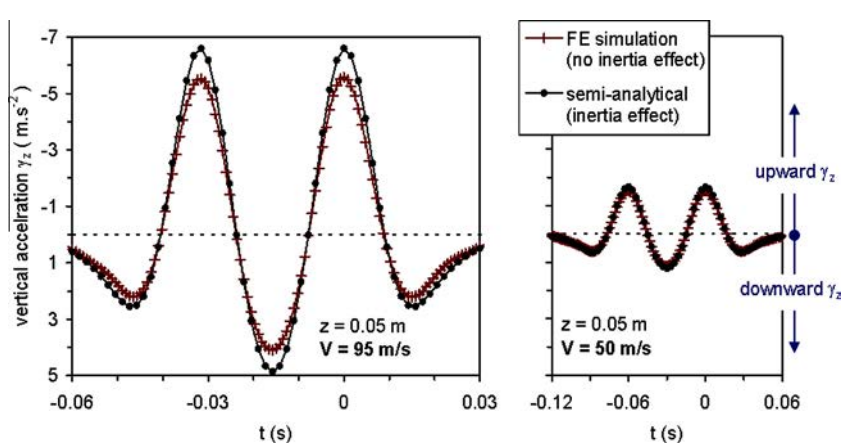

Fig. 10. Time evolution under a passing bogie ($V = 95$ and 50 m/s) of the vertical acceleration at the top of the ballast layer ($z = 0.05$ m) for a point located right under a sleeper center. Comparison between FE simulations without inertia effect and the semi-analytical method (full dynamics).

The effect of speed on γ_z could also be studied, viscoelastic materials being sensitive to the loading frequency. Moreover, other mechanical variables could be computed, in particular the extensional strains at the bottom of the asphalt layer since these are used in design criteria of such layers. However, such analyses are beyond the scope of the present paper and will be addressed in further works.

9. Conclusion

The goal of this study was to develop of a semi-analytical method for the computation of the dynamic response of railways including viscoelastic layers and solicited by moving loads. The developed method is based on a decoupling technique that consists in solving iteratively the two problems related to the rail/sleeper system and the trackbed. The connection between the two systems is made trough the vertical stress distribution under the sleepers which is decomposed into loading waves to make the rapid computation of the trackbed response in a quasi-stationary frame possible. The viscoelastic layers are modeled using the Huet–Sayegh thermo-sensitive viscoelastic law which gives access to an accurate modeling of the mechanical behavior of bituminous mixes. Therefore, the numerical method is well adapted to the simulation of railways incorporating asphalt layers as illustrated by the example presented in this paper.

Appendix A

Function. space that ensures constancy of loading at the surface of the structure

The aim of the present Appendix A is to derive the function space $f(x)$ such that

$$\sum_{n=-\infty}^{n=+\infty} f(x-n) = 1 \quad , \forall x \in \Re \tag{A1}$$

in which $\mathcal{R}$ is the set of real numbers. Let us assume that f has a Fourier transform $\hat{f}(s)$ defined as follows

$$\hat{f}(s) = \int_{-\infty}^{\infty} f(t)\, e^{-ist} dt \tag{A2}$$

in which s the transform variable. Then, based on Eq. (A1), we have

$$\sum_{n=-\infty}^{n=+\infty} TF(f(x-n))(s) = 2\pi\delta(s) \tag{A3}$$

with δ the delta Dirac distribution. TF stands for Fourier transform. On the other hand, term $\sum_{n=-\infty}^{n=+\infty} TF(f(x-n))(s)$ in Eq. (A3) can also be expressed as:

$$\sum_{n=-\infty}^{n=+\infty} TF(f(x-n))(s) = \hat{f}(s) \sum_{n=-\infty}^{n=+\infty} e^{-ins} \tag{A4}$$

Then, considering the distribution theory, it can be shown that the sum in the right hand side of Eq. (A4) is equal to

$$\sum_{n=-\infty}^{n=+\infty} e^{-ins} = 2\pi \sum_{n=-\infty}^{n=+\infty} \delta(s-2n\pi) \tag{A5}$$

Finally, combining Eq. (A3) with Eq. (A4) after substitution of Eq. (A5) into Eq. (A4) yields

$$\hat{f}(s) \sum_{n=-\infty}^{n=+\infty} \delta(s-2n\pi) = \delta(s) \tag{A6}$$

Interestingly n is not part of the argument of $\hat{f}$ and the function space that ensures Eq. (A1) can be summarized as follows

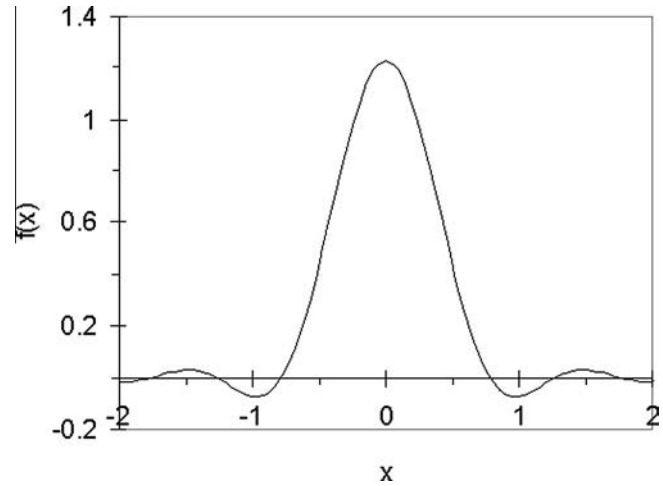

Fig. A1. Representation of the function given by (A9) for σ = 10.

$$\{\forall n \in Z^*, \hat{f}(2\pi n) = 0;\ \hat{f}(0) = 1\} \tag{A7}$$

in which Z^* is the set of integers with zero not included.

Example of a function satisfying Eq. (A6)

The following Fourier transform of function f satisfies Eq. (A7)

$$\hat{f}(s) = e^{-\frac{s^2}{2\sigma^2}} \cos\frac{s}{4} \quad \text{if} \quad s \in [-2\pi, 2\pi] \tag{A8}$$

$$\hat{f}(s) = 0 \quad \text{otherwise}$$

Thus, the inverse of Eq. (A8) is a function that could possibly be used as a master curve to define the loading at the surface of a railway structure. It reads:

$$f(x) = \frac{1}{2\pi} \int_{-2\pi}^{2\pi} e^{-\frac{s^2}{2\sigma^2}} \cos(sx) \cos\left(\frac{s}{4}\right) ds \tag{A9}$$

Obviously Eq. (A9) is more complicated than the Gaussian-type function used in the present article and it definitely would not be so easy to handle in the numerical computations. As an illustration, function $f(x)$ given by (A9) is represented for σ = 10 in Fig. A1.

References

Barros, F.C.P., Luco, J.E., 1994. Response of a layered viscoelastic half-space to a moving point load. Wave Motion 19, 189–210.

Chabot, A., Chupin, O., Deloffre, L., Duhamel, D., 2010. Viscoroute 2.0 a tool for the simulation of moving load effects on asphalt pavement. Road Mater. Pavement Des. 11, 227–250, No. 2/2010.

Chupin, O., Chabot, A., Piau, J.-M., Duhamel, D., 2010. Influence of sliding interfaces on the response of a layered viscoelastic medium under a moving load. Int. J. Solids Struct. 47 (3435–3446), 2010.

Chupin, O., Piau J.-M., 2011. Modélisation de la réponse dynamique d'une structure ferroviaire multicouche sous chargement roulant. 20ème Congrès Français de Mécanique, Besançon, France, 6 p.

Duhamel, D., Chabot, A., Tamagny, P., Harfouche, L., 2005. ViscoRoute: visco-elastic modeling for asphalt pavements. Bulletin des Laboratoires des Ponts et Chaussées 258–259, 89–103.

Filippov, A.P., 1961. Steady-state vibrations of an infinite beam on a elastic half-space under moving load. Izvestija AN SSSR OTN Mehanica and Mashinostroenie 6, 97–105.

Frýba, L., 1999. Vibration of Solids and Structures under Moving Loads, Noorhoff, Groningen, The Nederlands.

Hammoud, M., Duhamel, D., Sab, K., 2010. Static and dynamic studies for coupling discrete and continuum media; application to a simple railway track model. Int. J. Solids Struct. 47 (2010), 276–290.

Heck, J.V., Piau, J.M., Gramsammer, J.C., Kerzreho, J.P., Odeon, H., 1998. Thermovisco-elastic modelling of pavements behaviour and comparison with experimental data from LCPC test track. In: Proceedings of the 5th BCRA, Trondheim, Norway.

Huet, C., 1963. Etude par une méthode d'impédance du comportement viscoélastique des matériaux hydrocarbonés (Ph.D. Thesis). Université de Paris, France.

Metrikine, A.V., Popp, K., 1999. Vibration of a periodically supported beam on an elastic half-space. Eur. J. Mech. A Solids 18 (4), 679–701.
Rose, J.G., Teixeira, P.F., Veit, P, 2011. International design practices, applications and performances of asphalt/bituminous railway trackbeds. In: GEORAIL 2011: International Symposium, Paris, France, 19–20 May 2011.
Shannon, C.E., 1949. Communication in the presence of noise, Proc. Inst. Radio Eng. 37(1), pp. 10–21; Reprint as classic paper. In: Proceedings IEEE, 86(2), February 1998.
Sayegh, G., 1965. Contribution à l'étude des propriétés viscoélastiques des bitumes purs et des bétons bitumineux (Ph.D. Thesis). Faculté des Sciences de Paris, France.
Sheng, X., Jones, C.J.C., Petyt, M., 1999. Ground vibration generated by a load moving along a railway track. J. Sound Vib. 228 (1), 129–156.
Van den Broeck, P., Degrande, G., De Roeck, G., 2002. A prediction model for ground-borne vibrations due to railway traffic. In: Grundmann, H., Schuëller, G.I. (Eds.), Eurodyn 2002. Munich, Germany, pp. 503–508.
Vostroukhov, A.V., Metrikine, A.V., 2003. Periodically supported beam on a visco-elastic layer as a model for dynamic analysis of a high-speed railway track. Int. J. Solids Struct. 40, 5723–5752.
Zienkiewicz, O.C., 1971. The Finite Element Method in Engineering Science. McGraw-Hill, London.